High-Resolution Imaging with Multiparameter FWI for Land Data

James Sheng, Guanghui Huang, Terence Krishnasamy, Andrew Peterson, Mariana Gherasim, Jaime Ramos-Martínez and Carlos Calderón-Macías

Introduction

Full-waveform inversion (FWI) in land environments remains challenging due to several factors, including low signal-to-noise ratios at low frequencies, uncertainties in source-wavelet estimation, and the influence of surface topography. For shallow targets, limited near-offset coverage and strong near-surface heterogeneity often obscure primary reflections, reducing the effectiveness of conventional imaging algorithms (Reta Tang et al., 2023). Incorporating additional wavefield components beyond primary reflections can therefore play a critical role in improving illumination.

Although refracted energy is generally robust for velocity estimation, its depth of penetration is constrained by acquisition geometry—particularly maximum offset—as well as by the vertical velocity gradient. Beyond the depth limit sampled by refracted arrivals, FWI must rely predominantly on reflected energy. Effective background-velocity recovery from reflections, however, requires scale separation within the FWI gradient to achieve stable and efficient convergence.

In this study, we jointly invert for velocity and reflectivity using a multiparameter FWI (MP-FWI) formulation. The acoustic MP-FWI framework was introduced by Yang et al. (2021) and later extended to elastic media by Huang et al. (2025). Here, we adopt the acoustic formulation and incorporate the dynamic matching (DM) objective function (Huang et al., 2021) to enhance robustness, particularly at low frequencies. We first describe the methodology and then demonstrate its performance using a land seismic dataset from the Midland Basin.

Multi-Parameter FWI framework

The proposed MP-FWI framework consists of two fundamental components: a wave-equation parameterization in terms of P-wave velocity and reflectivity (Whitmore et al., 2020), and a scale-separation strategy that mitigates parameter crosstalk (Whitmore and Crawley, 2012; Ramos-Martinez et al., 2016). Parameterizing the wave equation with reflectivity eliminates the need for a density model to generate reflected energy for velocity updates. Given a smooth velocity model and an image, reflectivity modeling produces a full acoustic wavefield—including multi-scattering, free-surface effects, and refracted arrivals—in a single simulation. Applying scale separation to the FWI gradient yields two sensitivity kernels: a low-wavenumber kernel for velocity updates and a high-wavenumber kernel for reflectivity. The velocity kernel emphasizes background-velocity recovery from reflected energy beyond the penetration depth of refracted waves, while suppressing high-wavenumber leakage from reflectivity, particularly in the shallow subsurface. The DM objective function enhances phase alignment between observed and synthetic data through multidimensional cross-correlation. By reducing sensitivity to amplitude discrepancies and noise, it improves the robustness of the inversion in challenging land environments (Reta-Tang et al., 2023; Krishnasamy et al., 2023).

For reflectivity, using the full modeled wavefield significantly improves shallow-subsurface illumination compared with conventional imaging that relies solely on primary reflections. The reflectivity kernel enriches high-wavenumber content, and the iterative inversion recovers relative reflectivity amplitudes, leading to improved spatial resolution, enhanced image coherence, and reduced acquisition footprint.

Field Data Example

We applied the MP-FWI workflow to a land seismic dataset acquired with vibrator sources in the Midland Basin. The 3D survey spans approximately 692 km² and targets stratigraphic intervals including the Barnett Shale and Mississippi Lime. Maximum inline and crossline offsets reach roughly 7315 m. Data preprocessing steps included harmonic-noise attenuation, minimum-phase conversion,

low-frequency geophone-response compensation, high-amplitude noise suppression, ground-roll attenuation, and inverse-Q compensation.

The initial near-surface velocity model was constructed using refraction tomography, supplemented by sonic-log information where available (Figure 1a). This model was subsequently refined using DM-FWI and reflection tomography (Figure 1b). The lowest frequency used in FWI was 5 Hz. Velocity updates shown in Figures 2a and 2b illustrate the impact of scale separation: a conventional FWI gradient produces strong high-wavenumber updates tied to specular reflections, which typically require additional preconditioning and reflection tomography to recover the background velocity. In contrast, the velocity kernel isolates tomographic-scale updates within the same FWI framework, improving convergence of the background velocity model. The final inverted velocity model is presented in Figure 1c.

Figure 3 highlights the advantages of reflectivity inversion relative to RTM. Images were generated using the inverted velocity model, which is displayed as an overlay. The MP-FWI results exhibit improved focusing and spatial resolution, consistent with the depth slices shown in Figure 4. Channel definition is markedly enhanced in the MP-FWI images compared with the RTM results.

Conclusions

This study demonstrates the effectiveness of acoustic multiparameter full-waveform inversion for jointly estimating velocity and reflectivity in land seismic settings. Incorporating the dynamic matching objective function enhances the stability of velocity updates at low frequencies, where land data often suffer from low signal-to-noise ratios. Scale separation within the FWI gradient further improves the multiparameter inversion: the velocity kernel provides stable background-velocity updates in areas illuminated predominantly by reflected energy, while the reflectivity kernel enriches high-wavenumber content. Together, these components yield higher spatial resolution, improved image continuity, and overall superior imaging performance compared with conventional imaging approaches.

Acknowledgements

We thank TGS for authorization to publish this work and TGS Multiclient for providing the dataset. We thank our colleagues in TGS for fruitful discussions.

References

Huang, Y., Mao J., Sheng, J., Perz, M, He, Y., Hao, F., Liu, F., Yong, S.L., Chaikin, D, Ramirez, A, Hart, M. and Roende, H., 2023, Towards high-fidelity imaging: Dynamic Matching FWI: The Leading Edge, 42, 124-132.

Huang, G., Macesanu, C., Liu, F., Ramos-Martinez, J., Whitmore and Calderon, 2025, Multiparameter elastic FWI for joint inversion of velocity and reflectivity: 86th EAGE Conference and Exhibition, Extended Abstracts.

Ramos-Martinez, J., Crawley, S., Zou, K., Valenciano, A.A., Qiu, L. and Chemingui, N., 2016, A robust gradient for long wavelength FWI updates: 78th EAGE Conference & Exhibition, Extended Abstracts.

Reta-Tang, C., Sheng, J., Liu, F., Vazquez, A. and Cabrera, A., 2023, Applications of full waveform inversion to land data: case studies in onshore Mexico: The Leading Edge, 42, 190-195.

Krishnasamy, T., Sheng, J., Florendo, R., Beck, J., Sierra, A., Murphy, S., Siebens, J. and Iwo-Brown, Y., 2-023, High-resolution near-surface land FWI across the Delaware basin fill zone: 3rd International Meeting for Applied Geoscience & Energy Expanded Abstracts.

Whitmore, N.D., Ramos-Martinez, J., Yang Y. and Valenciano, A. A., 2020, Full wave field modelling with vector-reflectivity: 82nd EAGE Conference & Exhibition, Extended Abstracts.

Yang, Y., Ramos-Martinez, J., Whitmore, Huang, G. and Chemingui, N., 2021, Simultaneous inversion of velocity and reflectivity: First Break, 39(12), 55-59.

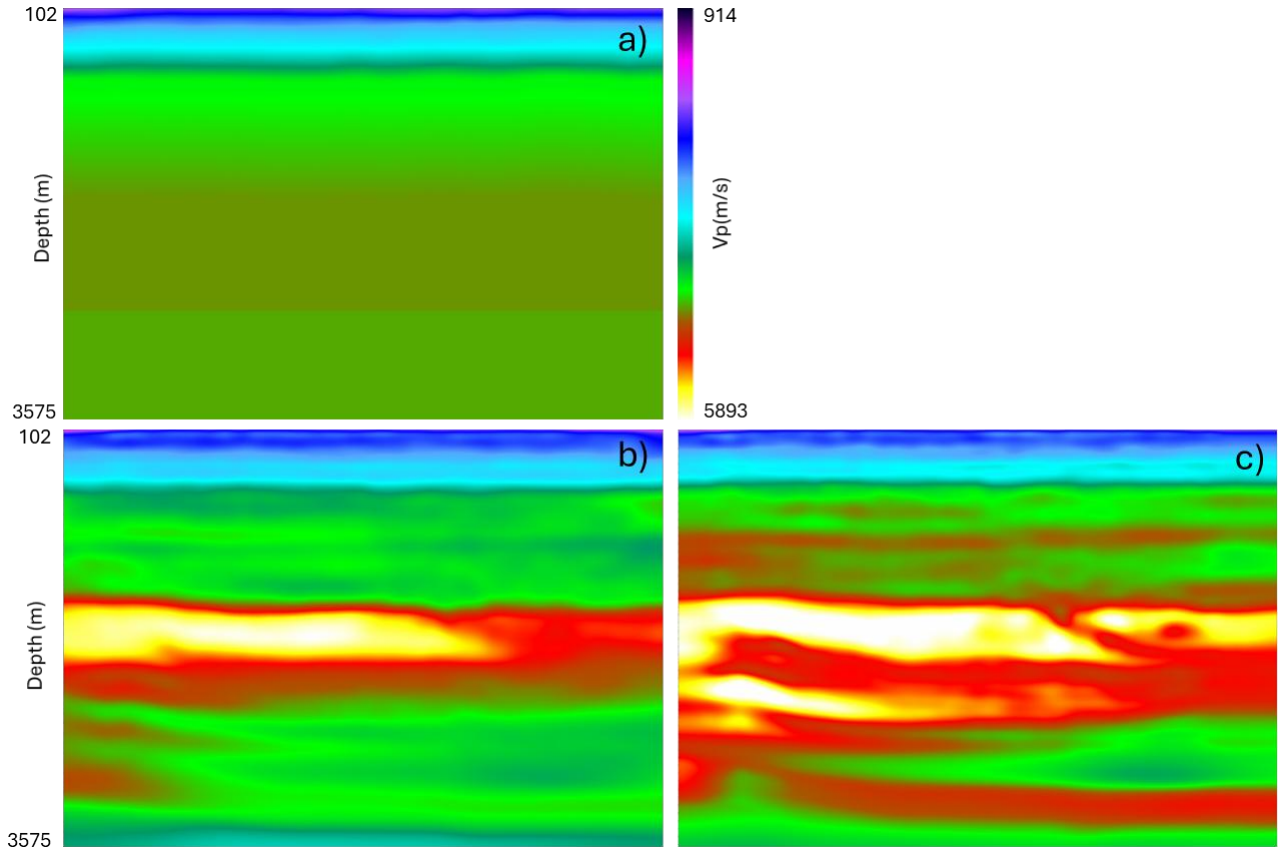

Figure 1. Midland basin example. a) Initial near-surface velocity model; b) intermediate velocity for MP-FWI; c) final inverted velocity model.

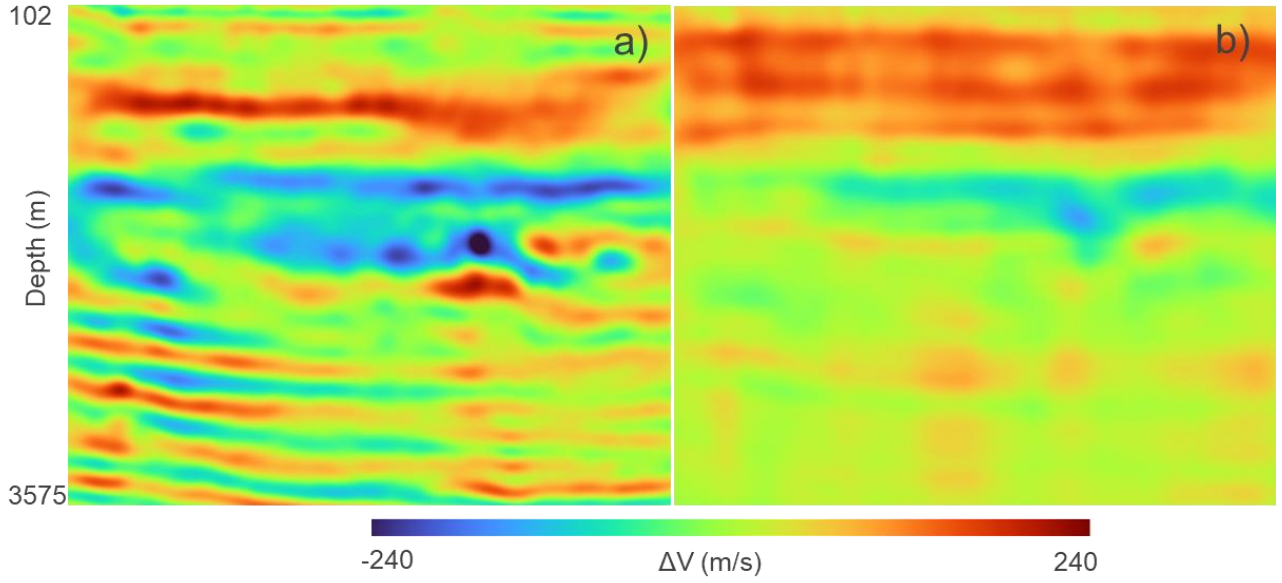

Figure 2. Midland basin example. Velocity updates using the a) conventional FWI gradient and b) the tomographic velocity kernel from MP-FWI.

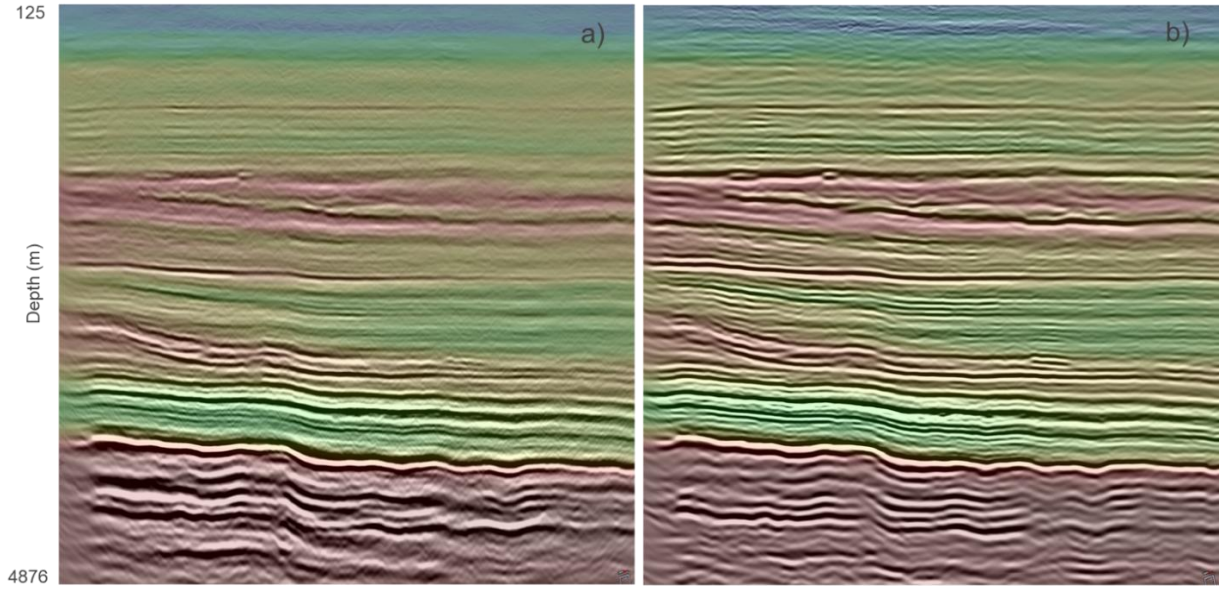

Figure 3. Midland basin example. a) RTM and MP-FWI reflectivity images along inline direction overlaying the inverted velocity model used in their construction (Figure 1c).

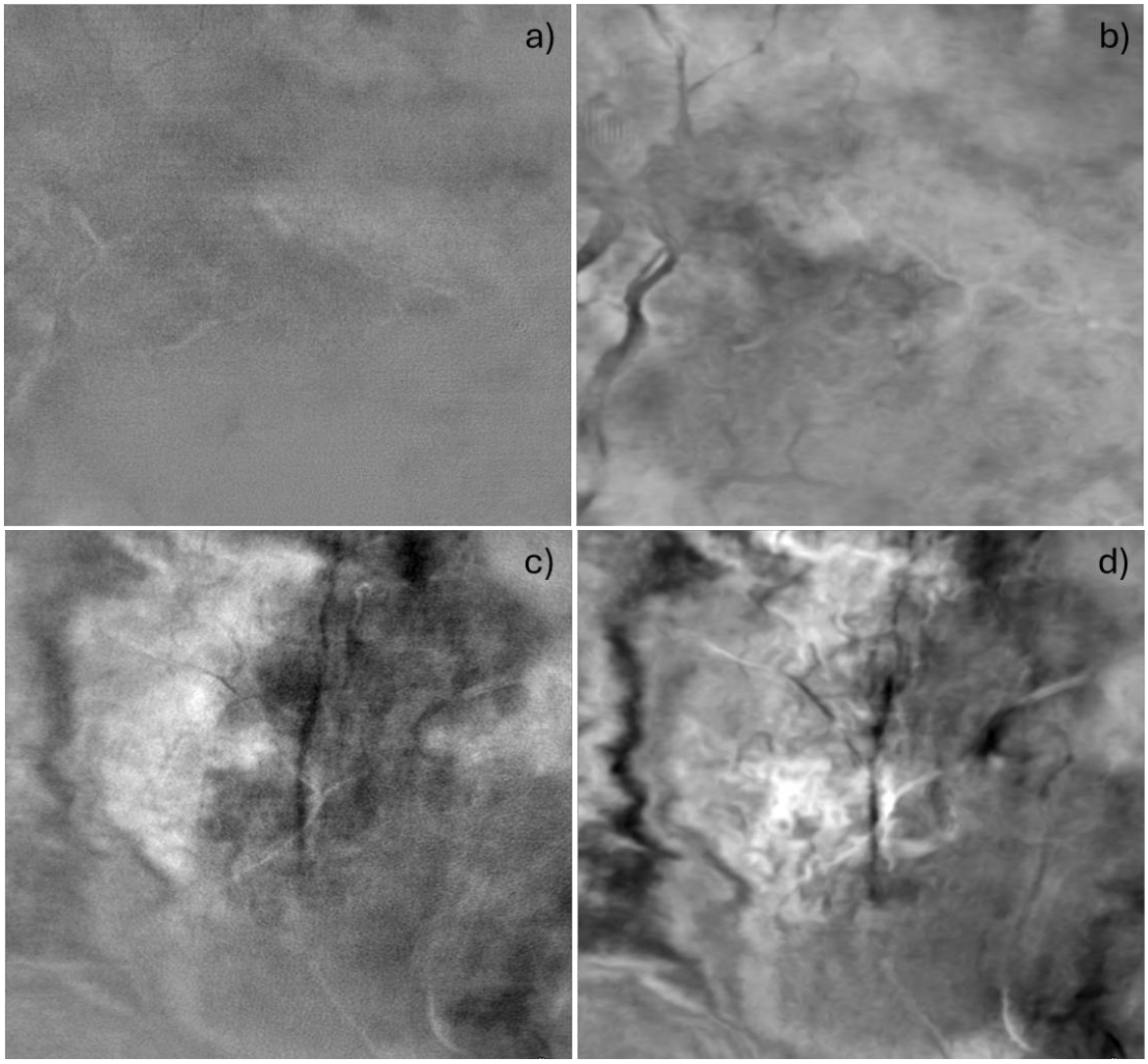

Figure 4. Midland basin example. a, c) RTM and b, d) MP-FWI reflectivity images for shallow (top) and intermediate (bottom) depths computed from the velocity model displayed in Figure 1c.